

Article

Polychrome Bronze Sculpture: A Multi-Analytical Approach to Unveil the Renaissance Gilded Eagles in the Abbey of San Miniato al Monte, Florence

Emma Cantisani ¹, Nicola Salvioli ² and Barbara Salvadori ^{1,*} 

¹ CNR-ISPC—National Research Council, Institute of Heritage Science, Via Madonna del Piano 10, Sesto Fiorentino, 50019 Florence, Italy; emma.cantisani@cnr.it

² Conservator, Restoration Firm, Viuzzo delle Canne 8R, 50136 Florence, Italy; info@nicolasalvioli.com

* Correspondence: barbara.salvadori@cnr.it; Tel.: +39-055-5225418

Abstract: The gilded bronze eagles that stand upon the summit of the Tabernacle by Michelozzo in the Abbey of San Miniato al Monte, Florence (Italy) are an exquisite example of Italian Renaissance sculpture. Commissioned by Piero di Cosimo de Medici, the two eagles, representing the ancient *Arte di Calimala*, were cast and decorated by Maso di Bartolomeo in the 1448–1449 period. A multi-analytical approach was set up to characterize the state of conservation, materials used, and artistic technique of the eagles. Non-invasive methods were used and integrated with micro-invasive analyses, such as X-ray fluorescence (XRF) and Fourier-transform infrared (FTIR) spectroscopy, X-ray diffractometry on powders (XRPD), scanning electron microscopy coupled with EDS (SEM-EDS), and metallographic investigation. The results depict shiny-looking eagles, suggesting the use of oil gilding on almost all surfaces and revealing the presence of polychromies, which is almost unusual in XV-century bronze statuary and is initially hidden by deposits and corrosion products. Indeed, the paws were originally painted with azurite, while the use of cinnabar imparted a vivid red color to the tongue. A black paint containing mercury was found on the eyes and talons. The bases of cloth were decorated with silver, which is now almost completely lost and whose remains are not visible due to being tarnished, while fine details in gold were detected on the lanyard.



Citation: Cantisani, E.; Salvioli, N.; Salvadori, B. Polychrome Bronze Sculpture: A Multi-Analytical Approach to Unveil the Renaissance Gilded Eagles in the Abbey of San Miniato al Monte, Florence. *Heritage* **2024**, *7*, 983–996. <https://doi.org/10.3390/heritage7020047>

Academic Editor: Vittoria Guglielmi

Received: 13 December 2023

Revised: 5 February 2024

Accepted: 6 February 2024

Published: 14 February 2024



Copyright: © 2024 by the authors. Licensee MDPI, Basel, Switzerland. This article is an open access article distributed under the terms and conditions of the Creative Commons Attribution (CC BY) license (<https://creativecommons.org/licenses/by/4.0/>).

Keywords: bronze sculpture; Renaissance; gilding; polychromies; non-invasive techniques; micro-invasive techniques

1. Introduction

From ancient Egypt to Greece, the search for color and light effects was pursued and then taken up and developed in Roman art, both in statuary and in everyday objects. The decoration of metals was achieved by combining different metals, like the early examples of variously colored gold alloys used for jewelry and purple-black patinated alloys containing gold, as well as by applying materials such as enamel, niello, glass, and stones or semi-precious stones [1]. The theme of polychromy in ancient statuary is rather challenging because the traces of the original colors are often modified by the natural processes of alteration, causing a loss of the original decorative effect as a result of pollution by previous cleaning interventions or colors being hidden by encrusted deposits. In recent years, interest in ancient polychromy has strengthened with new studies on stone [2–4], terracotta [5], and bronze statuary [6].

With regard to bronze, polychromy was obtained by means of surface finishes (patination with chemical treatments), metal inserts with the use of different alloys to achieve contrasting effects (anatomical and decorative parts), the application of paints, and gilding [6–8]. In the literature, there are several studies that report decorative techniques for bronze, including research on Egyptian, Etruscan, Greek, and Roman polychrome bronze objects and statuary [9–12]. Typical examples of colored copper-based alloys are the “black

bronzes” from the Hellenistic and Roman periods (Corinthian bronzes) [13]. However, although some studies investigate Italian Renaissance patination [14–18], to the authors’ knowledge, there are no references regarding polychrome bronze objects or statuary from this period. Over the centuries, gilding techniques have also been used to enhance the artistic value of metalworks, giving coloristic effects as well. Among them, foil and leaf gilding were widely used in antiquity, where the gold was fixed to the underlying metal either by mechanical action or with an animal or vegetable glue (oil gilding or “*doratura a missione*”) [19,20]. Fire gilding consisted of spreading a gold–mercury amalgam over the base metal or applying gold leaf to the substrate coated with mercury. In both cases, the application of the gold was followed by heating and burnishing to close the porous structure and give a smooth and reflective surface [21–23]. Unfortunately, the use of adhesives poses problems to the durability of the gilding due to the degradation and mineralization of the organic component, which often causes loss of the leaf, leaving only traces of gold caught in the folds and crevices of the object [24]. Fire gilding, instead, gives rise to a well-bonded layer of gold on the surface, thanks to copper–gold interdiffusion, which gives greater stability to the gilding [25].

As part of the celebrations for the millenary of the Abbey of San Miniato al Monte in Florence, held in 2018, an extensive restoration project was carried out, including the restoration of the bronze eagles that stand upon the summit of the marble tabernacle made by Michelozzo called “*Cappella del Crocifisso*”, placed in front of the entrance. Commissioned by Piero di Cosimo de Medici, the two eagles (approximately 42 cm high and 35 cm wide), clutching bales of cloth to represent the ancient *Arte di Calimala*, were cast and decorated by Maso di Bartolomeo from 28 January 1448 to 22 April 1449. Supported by the Friends of Florence Foundation, the restoration aimed to recover the legibility of the surfaces, bringing the original gilding affected by corrosion products, aged coatings, and disfiguring deposits back to its ancient splendor. Some details about the expenditures for lost-wax casting—“*le due aquile in ottone per mettere insu la Chappella de marmo. . .*”—can be found in the *Journal d’un sculpteur Florentin au XVe siècle* [26], where the prices of wood, wax, iron, and bronze are exactly reported.

Prior to restoration, the knowledge of execution techniques and the state of conservation of ancient artifacts is necessary for gaining awareness of historical and artistic value, as well as to set up appropriate intervention strategies. Due to the great artistic value of historic objects, the use of non-invasive portable instrumentation has gained significant interest in the last twenty years. Since non-invasive measurements do not require any contact with the examined object, they can be performed on the entire surface of interest, extending to a virtually infinite number of points with a clear advantage in terms of data representativeness. However, compared to the use of bench-top instruments dedicated to the analysis of samples or small objects, the application of portable and non-invasive techniques presents inevitable limitations, including problems of spectral interpretation of materials with multilayer character, as occurs in polychromies. In such cases, the application of a multi-analytical approach, where data derived from non-invasive and micro-invasive techniques are merged, is necessary to yield a more accurate characterization of materials and surface treatments [27]. The information obtained with the preliminary non-invasive study is also functional in guiding sampling, thus reducing the number and size of samples to the bare minimum.

With the aims of characterizing the artistic technique and the state of conservation of the two eagles from the Abbey of San Miniato al Monte and providing useful information for the restoration process (Appendix A), an in-depth diagnostic project was set up. An array of analytical techniques was employed, including non-invasive X-ray fluorescence spectroscopy (XRF), to map and identify the working technique of gilding on bodies and bales of cloth [28,29] with micro-invasive analyses. Regarding the powder samples taken from the surface, the compositions of pigments, deposits, and patinas were identified by combining Fourier-transform infrared (FTIR) spectroscopy [30] and X-ray diffractometry on powders (XRPD). The microstructure, composition of the alloys, and gilding techniques

were investigated on micro-fragments through the metallographic observation of cross-sections and scanning electron microscopy coupled with an EDS probe (SEM-EDS) [31].

2. Materials and Methods

The constituent materials, the manufacturing technique, and the state of conservation of the two gilt bronze eagles were determined by a combination of non-invasive investigations carried out on-site with portable instruments and micro-invasive laboratory analysis.

2.1. Non-Invasive Analyses

A Bruker Tracer III SD portable spectrometer equipped with a rhodium anode and a solid-state silicon detector energy dispersion system was used for the elemental analysis. Fifty spectra were recorded with a setting of 40 kV and 12 μ A and a measurement time of 60 s. In some points, the lines of the heavy elements were enhanced with a special filter (25.4 μ m copper, 25.4 μ m titanium, and 304.8 μ m aluminum). The penetration depth of the incident photons varies depending on their energy, the density of the sample, and the fluorescence energy of the chemical elements present in the material. In the case of lead-containing bronze alloys, it is estimated that 90% of the incident photons are absorbed in the first 100–200 μ m [32,33]. The ARTAX software was used for the data evaluation after the spectra had been normalized to the intensity of Rh Ka at 20.21 keV. All investigated areas were documented using a portable digital microscope with different magnifications (Scalar DG-2A, optical zoom 25–200 \times , magnification at 25 \times , area 13 mm \times 8 mm). Figure 1 shows the location of the XRF measurement points on the eagles and bales of cloth.

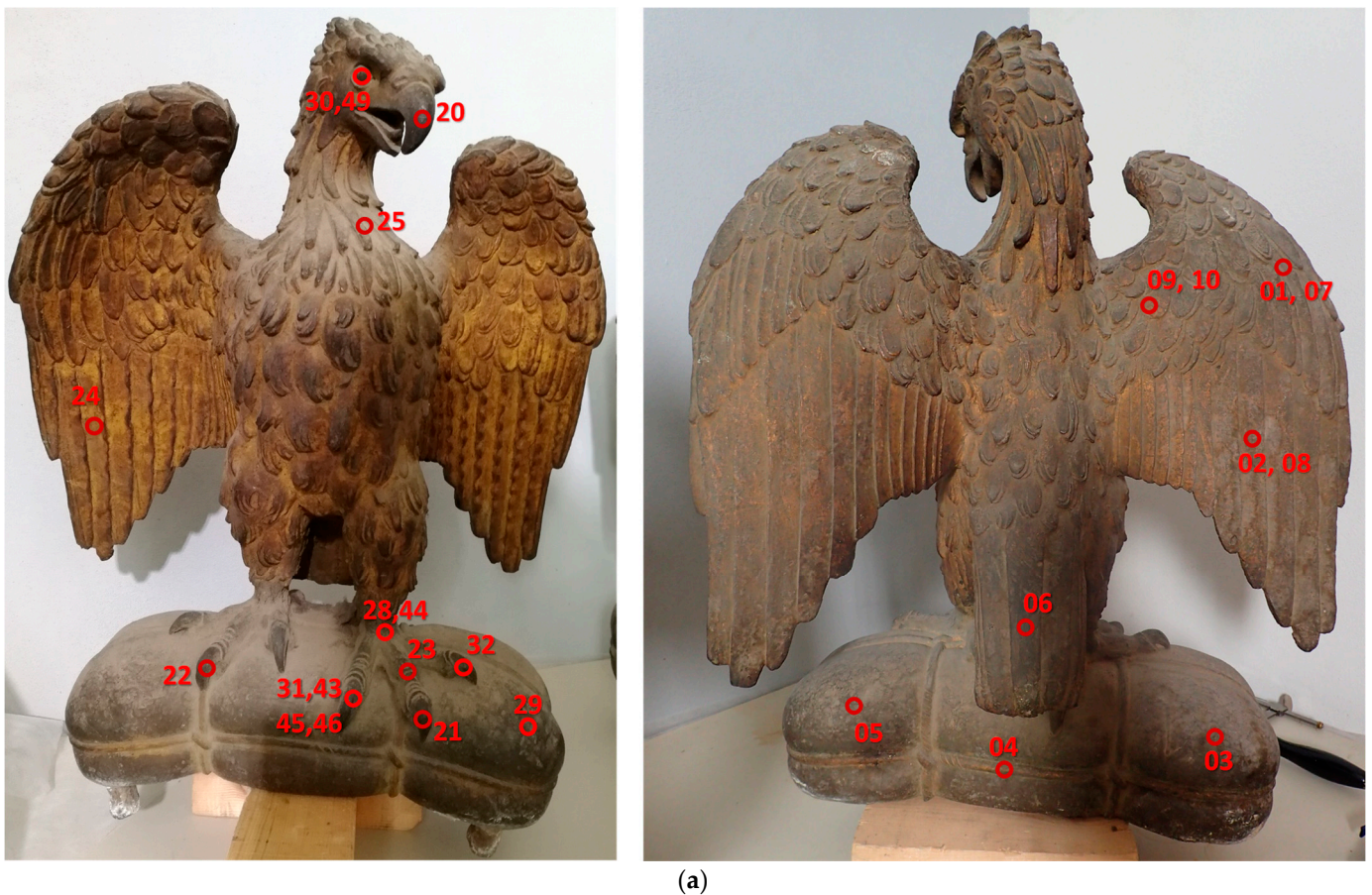


Figure 1. Cont.

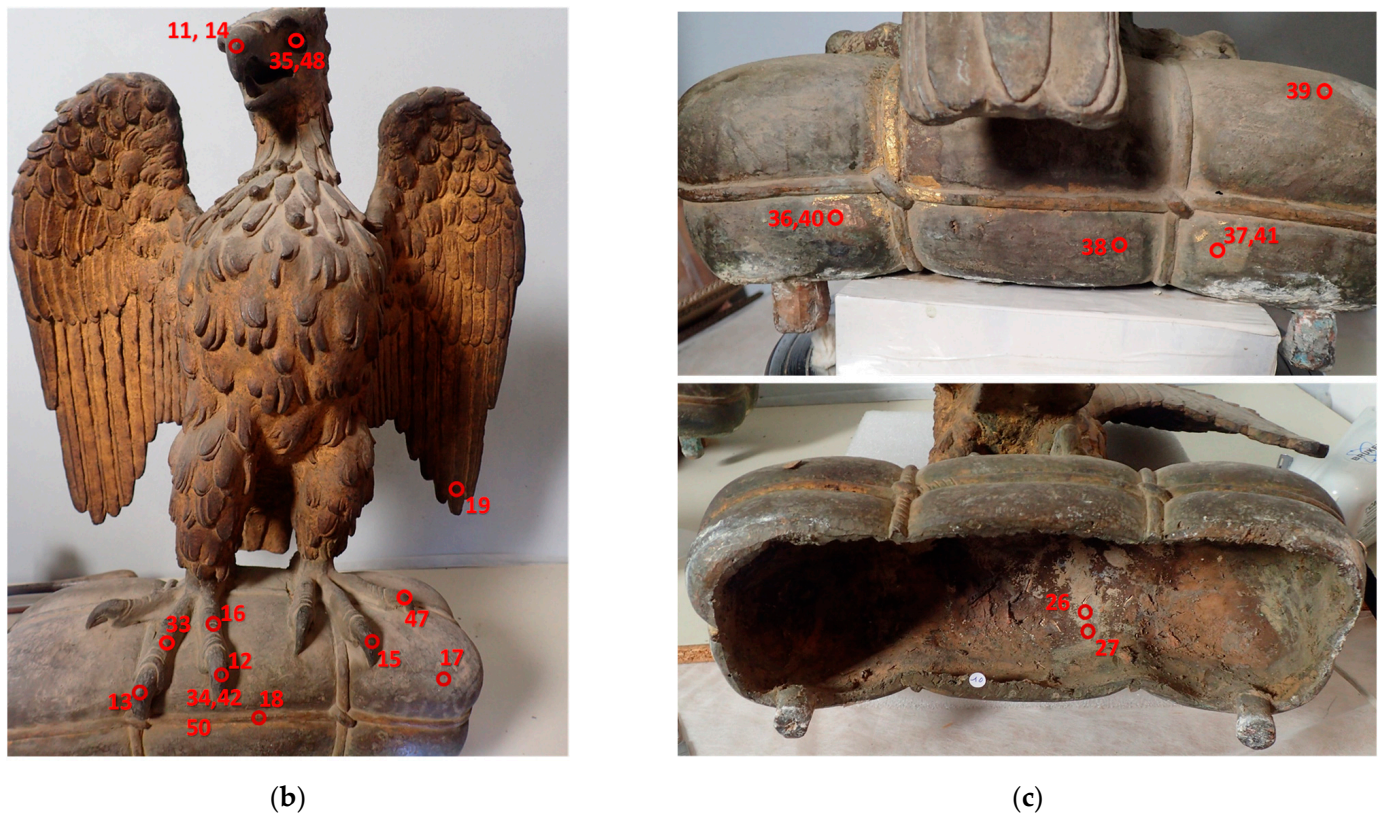


Figure 1. Location of the XRF measurement points of analyses. (a) Eastern eagle; (b) Western eagle; (c) bales of cloth under the Western (top) and Eastern eagles (bottom).

2.2. Micro-Invasive Analyses

2.2.1. Samples

Powders (a few mg) of deposits and of corrosion patina, as well as micro-fragments that include patina, gilding (if present), and alloy, were taken to characterize the composition and microstructure. Figure S1 shows the sampling points and the associated powders and fragments. Samples 11–14 were taken from the areas of interest after the cleaning tests. Table 1 contains a brief description of the samples analyzed and the applied methods.

Table 1. Samples taken from the two statues and the analytical methods used.

Sample	Type of Sample	Position	Description	Analytical Techniques
01	Chip	Western eagle, tail	stratigraphic sample	Metallography; SEM-EDS
02	Chip	Western bale of cloth	stratigraphic sample	Metallography; SEM-EDS
03	Powder	Western bale of cloth	green patina	ATR-FTIR; XRPD
04	Powder	Western bale of cloth	hard deposit	ATR-FTIR; XRPD
05	Powder	Western bale of cloth	hard deposit	ATR-FTIR; XRPD
06	Powder	Western eagle, under the tail	green patina	ATR-FTIR; XRPD
07	Powder	Western eagle, on the gilding	whitish patina	ATR-FTIR
08	Powder	Western eagle, feather	dark patina	ATR-FTIR
09	Chip	Eastern eagle, under the wing	stratigraphic sample	Metallography; SEM-EDS
10	Chip	Eastern bale of cloth	stratigraphic sample	Metallography; SEM-EDS
11	Powder	Western eagle, on the paw	blue paint	ATR-FTIR; XRPD
12	Powder	Western eagle, from the talon	black paint	ATR-FTIR; XRPD
13	Powder	Eastern eagle, from the talon	black paint	ATR-FTIR; XRPD
14	Powder	Western eagle, on the tongue	red paint	ATR-FTIR; XRPD

2.2.2. FTIR Spectroscopy

The powders were analyzed using an Agilent Technologies Cary 660 FTIR spectrometer coupled with a Cary 620 Microscope equipped with an MCT detector. All spectra were recorded in microATR mode with germanium crystal, 64 scans, and a resolution of 4 cm^{-1} in the $4000\text{--}400\text{ cm}^{-1}$ range. The spectra were processed using Agilent Resolutions Pro software.

2.2.3. XRPD

X-ray powder diffraction (XRPD) was used to determine the crystalline composition of patinas and deposits. An X'Pert Pro PANalytical powder X-ray diffractometer (Cu anticathode ($\lambda = 1.54\text{ \AA}$)) was used under the following conditions: current 30 mA, voltage 40 kV, explored 2θ range between 3 and 70° , and step size 0.02° . A zero-background sample stage was used. The Powder Diffraction (PDF) database of the International Center for Diffraction Data (ICDD) was used for the phase identification of the XRPD results.

2.2.4. Optical Microscopy (MO) and Scanning Electron Microscopy (SEM-EDS)

The microstructure and composition of the alloy were examined on cross-sections by metallographic observation and scanning electron microscopy coupled with an EDS probe (SEM-EDS), respectively. All samples were first observed using a Zeiss Stemi 200 C stereomicroscope equipped with a high-resolution photo camera. Samples 01, 02, 09, and 10 were embedded in epoxy resin, cut perpendicular to the stratigraphy, and polished with sandpaper (180 to 4000 grit) and diamond paste (6 to $1\text{ }\mu\text{m}$) to obtain the cross-sections. Observations were made with an optical microscope in visible and ultraviolet-reflected light using a Nikon Eclipse E600 microscope equipped with a halogen lamp (12 V, 100 W) with fiber optics and a mercury vapor lamp for the UV fluorescence observations. The objectives used were $1\times$, $4\times$, $10\times$ and $20\times$. The acquisition and processing software is Nikon ACT-1. For the metallography, the observation was repeated before and after the attack with the FeCl_3/HCl reagent [34]. The cross-sections were also observed and analyzed by SEM-EDS. A ZEISS EVO MA15, equipped with EDS and OXFORD INCA 250 software, operates at a 20 kV acceleration voltage, 700 pA emission current, and a working distance of 9.5 mm.

3. Results

3.1. X-ray Fluorescence Spectroscopy (XRF)

The elements detected on each measurement point are listed in Table S1. Gold signals were detected at all examined points on the body of the eagles (Figure 2a), but not on the paws and talons (Figure 2b). The beak also showed significant gold values (Figure 2c). Gold signals were also found on the lanyard of the bale of cloth but not on the bale itself (Figure 2d). Instead, silver was detected at all measurement points on the bales of cloth (spots 03, 05, 17). When using the filter to enhance the detection of the heaviest metals (Section 2.1), weak lines attributable to silver were also found on the parts of the talons closest to the bales, probably due to the size of the silver leaves applied to the bales' surface, which partially overlapped with the eagle's body. Mercury was found on the black-painted talons and eyes of the Western eagle, while gold was absent (Figure 2b). Instead, no mercury was detected on the Eastern eagle.

The presence of copper, tin, and antimony signals was ubiquitous and attributable to the underlying bronze alloy. Arsenic signals were detected on the bale of cloth, together with silver (Figure 2d). Weak arsenic signals were also observed in correspondence with some points on the talons and paws. Lead was also detected.

Small amounts of manganese were attributed to impurities in the alloy, while potassium, silicon, calcium, and sulfur were due to atmospheric deposition. In the Eastern eagle, a dot of red paint on the right wing (points 01, 07) consists of mercury and sulfur (cinnabar).

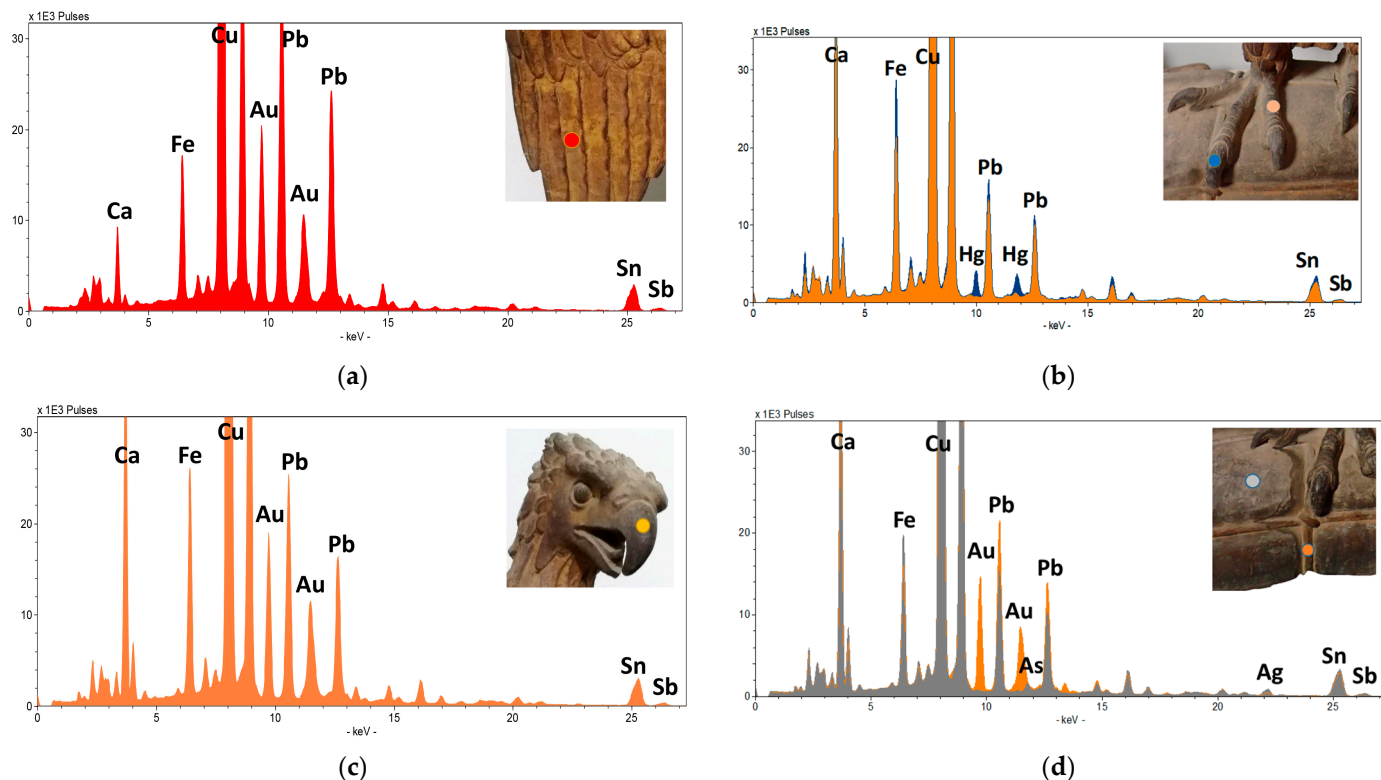


Figure 2. XRF spectra of (a) point 24 on one of the feathers of the Eastern eagle; (b) points 13 (orange) and 16 (blue) on the paw and talon of the Western eagle, respectively; (c) point 20 on the beak of the Eastern eagle and (d) points 03 (orange) and 04 (gray) on the bale of cloth of the Eastern eagle and lanyard, respectively.

3.2. Fourier-Transform Infrared Spectroscopy (FTIR) and X-ray Powder Diffraction (XRPD)

Figure 3a shows representative FTIR spectra of samples 06, 08, and 11. The composition of the deposits and patina detected by ATR-FTIR and XRPD analyses is summarized in Table 2, while the main FTIR vibrational bands of the detected compounds and their assignments are listed in Table S2 [35–48]. The XRPD patterns are shown in Figure S2. The complementarity of XRPD and FTIR made it possible to characterize the organic and inorganic compounds in the samples. Apparently, different results between the two analytical techniques are either due to the fact that FTIR can identify amorphous compounds that are not detectable by XRPD or due to the different sizes of the analyzed sample (whole powder for XRPD, selected grains for ATR-FTIR).

Silica-based deposits (quartz and other silicates), gypsum ($\text{CaSO}_4 \cdot 2\text{H}_2\text{O}$), calcium carbonate (CaCO_3), and weddellite (calcium oxalate, $\text{CaC}_2\text{O}_4 \cdot 2\text{H}_2\text{O}$) were detected in the powders analyzed before cleaning (samples 04 and 05). In the green patina, either atacamite (copper hydroxychloride, $\text{Cu}_2\text{Cl}(\text{OH})_3$) or gerhardtite (basic copper nitrate, $\text{Cu}_2(\text{NO}_3)(\text{OH})_3$) were detected, as well as cuprite (cuprous oxide, Cu_2O) in samples 03 and 13. In samples 06 and 13, nantokite (copper chloride, CuCl) was detected in the XRPD analyses. Calcium and copper (moolooite, $\text{CuC}_2\text{O}_4 \cdot \text{H}_2\text{O}$) oxalates were also detected in the patina, which can be attributed to the degradation (mineralization) of the protective agents applied in the past [49]. Sample 06 also shows some bands between 2955 and 2850 cm^{-1} assigned to $\nu_{\text{as}}(\text{CH}_3)$ and $\nu_{\text{s}}(\text{CH}_2)$, suggesting an organic material. Instead, the weak band at 1412 cm^{-1} can be attributed to a carbonate, which is consistent with the XRPD results. The blue paint on the paw (sample 11, Figure 3a) under the wing of the Western eagle is composed of azurite ($2\text{CuCO}_3 \cdot \text{Cu}(\text{OH})_2$) and a proteinaceous substance that was probably used as a binder for the pigment, while silica-based deposits and alteration products, such as copper oxalate and lead sulfate (PbSO_4), were also found. The red paint on the tongue (sample 14) contains gypsum, calcium oxalate, silicates, and gerhardtite, as well as cinnabar

(HgS). On the Eastern eagle, after cleaning, polysaccharide compounds were found in the black paint (sample 13) together with nantokite, cuprite, hematite (Fe_2O_3), silicates, tenorite (CuO), and gypsum. ATR-FTIR analysis of small fragments of gilding (sample 08, Figure 3a) showed the presence of a lipid compatible with an oil binder, as well as moolooite and gypsum (see Table S2 for vibration band assignments). MicroATR-FTIR analysis of the layer visible under the gold further revealed vibrational bands associated with ester-type substances: $\nu_{\text{as}}(\text{CH}_3)$ and $\nu_{\text{s}}(\text{CH}_2)$ at 2928 and 2858 cm^{-1} , respectively; $\nu(\text{C}=\text{O})$ at 1710 cm^{-1} , and antisymmetric and symmetric $\nu(\text{COO}^-)$ vibrations and $\delta(\text{CH}_2)$ between 1615 and 1406 cm^{-1} (Figure 3b), compatible with a mixture of drying oil and metal carboxylates [42–44,50].

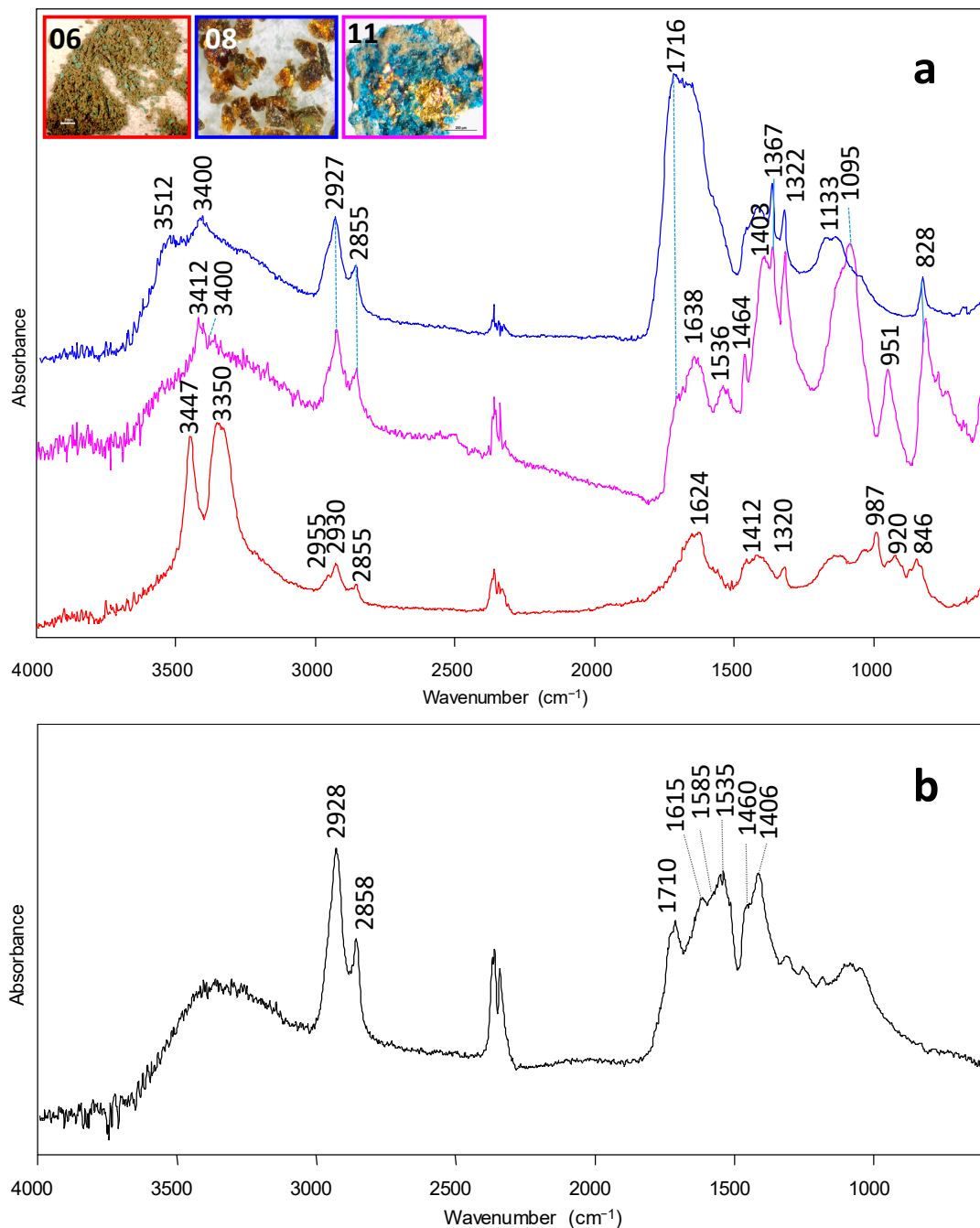


Figure 3. (a) FTIR spectra of samples 06, 08, and 11 analyzed in ATR mode; (b) microATR-FTIR spectrum of the layer under the gilding.

Table 2. Composition of the deposits and patinas determined with ATR-FTIR and XRPD. W: Western eagle; E: Eastern eagle; B: bale of cloth.

Sample	Description	Position	ATR-FTIR	XRPD
03	Green patina	W, B	Organic material, calcium carbonate	Cuprite, gerhardtite
04	Deposit	W, B	Gypsum, calcium oxalate, calcium carbonate, silicate	Gypsum
05	Deposit	W, B	Gypsum, calcium oxalate, calcium carbonate, silicate	Gypsum
06	Green patina	W	Atacamite, calcium oxalate, calcium carbonate	Atacamite, calcite, quartz, nantokite, paratacamite, weddellite, gypsum
07	White patina	W	Calcium oxalate, silicate	n.a.
08	Patina	W	Moolooite, gypsum, oil binder	n.a.
11	Blue paint on paw, after cleaning	W	Azurite, copper oxalate, oil binder, proteinaceous substance	Azurite, gold, lead sulphate
12	Dark paint on talon, after cleaning	W	Atacamite, calcium oxalate, moolooite	Weddellite, gypsum, quartz
13	Dark paint on talon, after cleaning	E	Polysaccharide component	Nantokite, cuprite, hematite, quartz, tenorite, gypsum
14	Red paint on tongue	W	Gypsum, calcium oxalate, moolooite, silicate	Cinnabar, gerhardtite, gypsum

3.3. Optical Microscopy (OM) and Scanning Electron Microscope Coupled with Energy Dispersive Spectroscopy (SEM-EDS)

The SEM-EDS analysis of the alloys of the body and bale of cloth of the Western eagle (samples 01 and 02, respectively) is shown in Figure S2. A binary Cu-Sn alloy (spectrum 1) with a few small lead globules was detected (spectrum 2) in the body. Impurities of silicon and aluminum were also detected in traces (spectrum 3), as well as antimony (spectrum 4). In the Cu-Sn alloy of the bale of cloth (spectrum 2), an Sn-enriched intergrain eutectoid phase was found in addition to small lead globules (spectrum 3) and antimony-containing inclusions (spectrum 1,4). These results are similar to those obtained in the corresponding parts of the Eastern eagle (samples 09 and 10, respectively). The elemental composition of each sample is reported in Table 3.

Table 3. Elemental composition from SEM-EDS analyses of samples taken from the Western (01,02) and Eastern eagles (09,10).

Sample	Description	Eagle	O wt%	Si wt%	Cu wt%	Sn wt%	As wt%
01	Body	W	2.55	0.85	88.85	8.15	
02	Bale of cloth	W	2.72		89.74	7.54	
09	Body	E	2.24		89.56	8.23	
10	Bale of cloth	E	2.62		87.99	9.08	0.63

In both sculptures, the metallographic analyses (Figure 4) revealed a dendritic microstructure with the α -phase partially homogenized, probably due to moderate heating. The surface grains were flattened, suggesting that the object had been cold-worked. Strain lines were also visible along the thickness of the sample, suggesting an intense mechanical process due to heavy hammering.

Figure 5 shows the stratigraphy on the cross-section of the body of the Western eagle (sample 01), which is also representative of that of the Eastern eagle (sample 09, SEM images not reported). From bottom to top, the observations in bright-field (Figure 5a) and UV light (Figure 5b) show the following: (i) alloy; (ii) organic fluorescent layer (10–30 μm thick); (iii) gold leaf (about 2 μm thick); and (iv) superficial patina composed of deposits and corrosion products. SEM-EDS analyses (Figure 5c) showed the Cu-Sn alloy (layer (i),

Figure 5d) under a lead-rich layer with minor amounts of iron, calcium, potassium, silicon, magnesium, and chlorine (layer (ii), Figure 5e). The gold leaf (layer (iii), Figure 5f) consists of pure gold. Silicon, aluminum, potassium, and chlorine were detected in the superficial patina (layer (iv), Figure 5g).

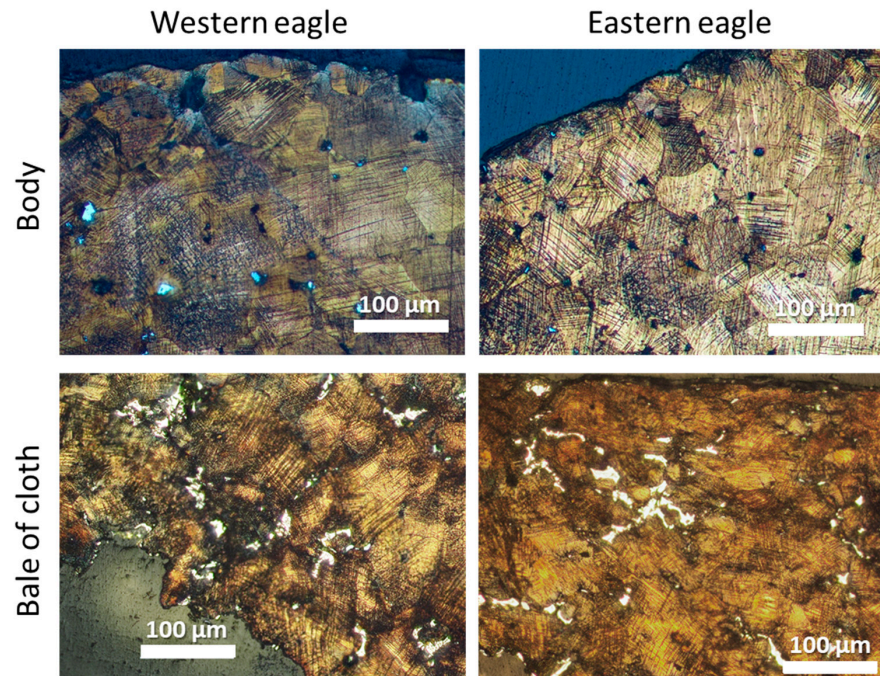


Figure 4. Metallographic examination of sample 01, sample 09 (body) and sample 02, and sample 10 (bale of cloth) from Western and Eastern eagles, respectively.

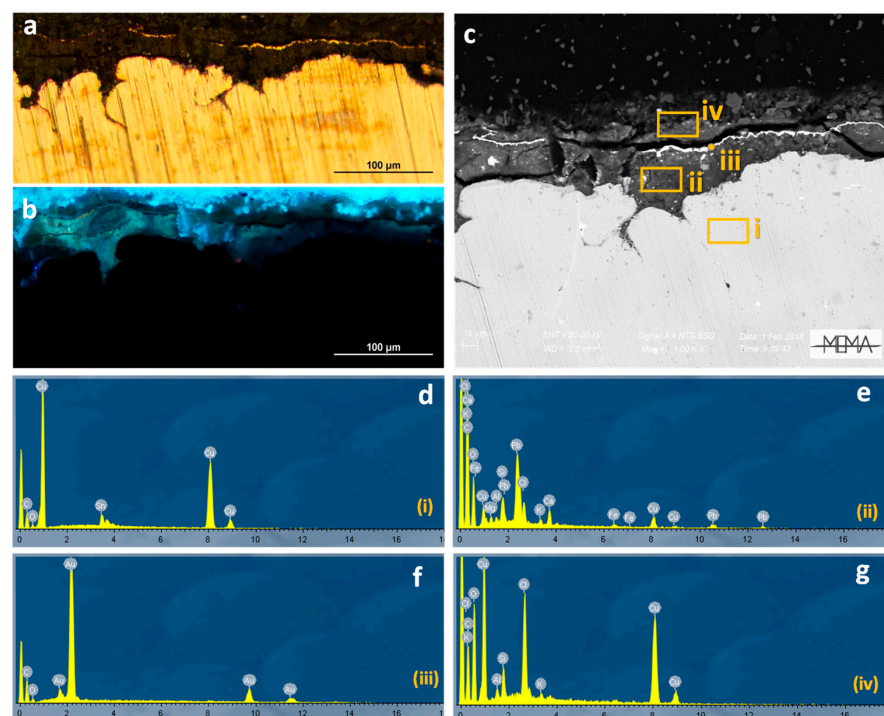


Figure 5. (a) Optical microscope observation in visible and (b) UV light of the cross-section of sample 01 (Western eagle); (c) SEM-EDS backscattered electron image with EDS spectra of (d) alloy—layer (i); (e) adhesive for gold leaf—layer (ii); (f) gold leaf—layer (iii); and (g) patina—layer (iv).

4. Discussion

The preliminary non-invasive measurements with a portable XRF device proved to be effective, not only for mapping the gilding and hypothesizing its execution technique but also for detecting decorations and polychromies that are not clearly visible under the patina of time. The results of the XRF also guided the later sampling necessary to better study the alloys and compounds using laboratory techniques.

Most of the surface of the eagles was originally gilded with a thin leaf (approx. 2 μm thick), as evidenced by the detection of gold at almost all points of the XRF measurement and confirmed by cross-sections. The absence of mercury in the areas where gold is present suggests that the leaf-gilding technique was used and not amalgam. The detection of FTIR vibrational bands related to lipids indicates the presence of a siccativ oil in the layer beneath the gold, further supporting the oil-gilding hypothesis. Metal carboxylates were also detected, probably originating from the reaction of the oil with the alloy and/or with metal ions in the minerals contained in the sizing. Lead was also found in the cross-sections using SEM-EDS and was attributed to lead white (basic lead carbonate, $2\text{PbCO}_3 \cdot \text{Pb}(\text{OH})_2$), which is usually added to the mixture to improve the setting of the oil and/or to lighten the color. This layer was infiltrated by chloride-based corrosion products and contained clay minerals, as suggested by the detection of chlorine and typical earth elements (aluminum, silicon, iron, magnesium, and potassium), respectively.

The bales of cloth were originally decorated with silver, as the detection of this element on the entire surface of both bales suggests, while it is missing in the alloy. However, the decoration seems to have been largely lost, as can be deduced from the weak intensity of the silver signals. Instead, the lanyards were gilded, as evidenced by the presence of gold. The weak silver signals detected on the gilded Eastern lanyard can be attributed to the overlapping of gold and silver leaves. The arsenic found in very small amounts together with silver, as well as in some points on the paws and talons near the bale of cloth [16,21,22], may indicate impurities that were not completely removed from the ore by smelting [51]. Nevertheless, traces of arsenic are frequently found in Renaissance bronzes [52].

The chemical composition of the alloy is quite homogeneous, 88–90% copper and 7–9% tin, quite typical of Renaissance bronzes [53]. Small lead globules and traces of antimony were also detected in the bodies and bales of cloth, which can be attributed to impurities.

The microstructure of the alloy is compatible with that of a dendritic Cu-Sn binary bronze that has been subjected to moderate heating and subsequent cold working, as suggested by the strong strain lines and the flattening of the surface phases. The eutectoid phase, which is rich in tin, is particularly evident in the bales of cloth, whereas it is hardly present in the eagle bodies. Given the similar composition of the alloy, this difference in microstructure may indicate faster cooling of the bales of cloth compared to the bodies [53].

The surface deposits consisted of gypsum, calcium carbonate, and silicates, as well as alteration products of the alloy (atacamite and gerhardtite) and of protective agents used in the past (copper and calcium oxalates).

Nantokite was also found (Western and Eastern eagles, samples 06 and 13, respectively), which is considered a precursor of bronze disease [8] and must, therefore, be regarded as a warning signal for the activation of cyclic corrosion processes. A polysaccharide material was also found, which is probably due to contamination.

The analysis of micro-samples taken from the surface revealed the presence of azurite on the paws of the eagles and of cinnabar on the red tongues. The red dot composed of mercury and sulfur on the plumage of the Eastern eagle may be related either to incidental or intentional marking with cinnabar.

Regarding the black paint on the talons and eyes, the absence of characterizing elements and compounds could suggest the use of carbon black. Nonetheless, in the black paint on the Western eagle, mercury was detected, but the absence of any Hg-based compounds (as shown in Table 2, sample 12) makes this finding not clearly interpretable. Several studies discuss the well-known instability of red cinnabar ($\alpha\text{-HgS}$) and the influence of light, chloride ions, and humidity in the degradation of this pigment to chlorinated

compounds, black β -HgS, or metallic mercury [54,55]. However, the Eastern eagle did not show any evidence of mercury, and the absence of any pigment or compound consistent with the presence of this element in the sample from the Western eagle's talon still leaves this issue open.

The results of the analytical examination have allowed us to hypothesize the original polychromy of the eagles. In addition to the thin gold-leaf coating, which has been almost completely preserved under the concretions thanks to the location indoors, it can be assumed that the eagles originally sported red-dyed tongues, black-colored eyes, and talons and azurite-blue paws, while the bales of cloth shone with the silver–gold contrast of cloth and lanyard. Figure 6a and b show the evolution of the surfaces as a result of the restoration intervention, during which the decorations and pigment residues were rediscovered; Figure 6c shows the digital reconstruction of the original polychromy.



Figure 6. Eastern eagle (a) before, (b) after cleaning, and (c) after digital reconstruction of polychromy derived from the results of the scientific analyses.

5. Conclusions

This study confirmed the validity of a two-stage, multi-analytical approach based on the combination of non-invasive and micro-invasive techniques, in which the former guides the selection of micro-samples for an in-depth investigation of complex issues.

The results of this multi-analytical approach provided important information both for the art-historical knowledge of a rare example of a painted bronze statue from the Renaissance and for the cleaning intervention. The use of oil gilding was confirmed on almost the entire body, including the beak, and a partial polychromy was revealed that is almost unique to XV-century bronze statues and was initially obscured by the patina of time. The paws were originally painted with azurite blue, while the use of cinnabar gave the tongue a bright red color. Black paint was found on the eyes and talons, probably based on carbon black and containing mercury, the origin of which is an open question. XRF revealed silver foil on the bale of cloth, which is now tarnished, while fine details in gold were detected on the lanyard.

Supplementary Materials: The following supporting information can be downloaded at: <https://www.mdpi.com/article/10.3390/heritage7020047/s1>, Figure S1: Sampling points and corresponding samples (powders and fragments) observed under stereomicroscope; Table S1: For each XRF point of analysis, elements detected and detail of the analyzed surface; Table S2: Main vibration bands detected in the samples taken from the eagles, with their assignments; Figure S2: XRPD patterns; Figure S3: SEM-EDS analysis of the alloy of samples 01 (body) and 02 (bale of cloth) from the Western eagle. References [35–48] are cited in the Supplementary Materials.

Author Contributions: Conceptualization, B.S. and E.C.; methodology, B.S.; validation, B.S.; formal analysis, B.S. and E.C.; investigation, B.S. and E.C.; resources, B.S., E.C. and N.S.; data curation, B.S.; project administration, B.S.; writing—original draft preparation, B.S. and E.C.; writing—review and editing, B.S., E.C. and N.S.; project administration, B.S.; funding acquisition, B.S. and N.S. All authors have read and agreed to the published version of the manuscript.

Funding: This research received no external funding.

Data Availability Statement: The datasets used and analyzed during the current study are available from the corresponding author upon reasonable request.

Acknowledgments: The authors wish to thank Bernardo Gianni, abbot of the San Miniato al Monte Abbey, for his kind permission to disseminate the results. The Friends of Florence Foundation is gratefully acknowledged for their financial support of the restoration. Thanks are also due to Laura Chiarantini (University of Florence) for her precious suggestions on the interpretation of alloy microstructures and for her assistance in the SEM-EDS analyses at the Centro di Servizi di Microscopia Elettronica e Microanalisi (MEMA), University of Florence.

Conflicts of Interest: The authors declare no conflict of interest.

Appendix A

The encrusted deposits and remnants of previous treatments were removed from the surface using a combination of laser ablation and chemical cleaning. A Nd:YAG laser with a Long Q-switched pulse was used [56]. For the paws and talons, water solutions with agar gel were used, which were alternately washed with mild solvents to preserve the paint residues. Both cleaning methods were used for the bales of cloth and then finished by delicate mechanical action with a scalpel. Figure A1 shows the detail of the cleaning result, revealing the blue polychromy of the paws, which was originally obscured by the encrustations of dirt and corrosion products of the alloy.



Figure A1. (a) Thick encrustations obscuring the surface texture on the talons, and (b) polychrome details and gilding revealed by cleaning.

References

1. Giunlia-Mair, A. Polychromy on Greek and Roman Metals: Text and analyses. In Proceedings of the III Workshop des Netzwerks Archäologisch-Historisch es Metallhandwerk, Über den Glanz des Goldes und die Polychromie, Berlin, Germany, 11–12 May 2017.
2. Magrini, D.; Bracci, S.; Bartolozzi, G.; Iannaccone, R.; Lenzi, S.; Liverani, P. Revealing Mithras' Color with the ICVBC Mobile Lab in the Museum. *Heritage* **2019**, *2*, 2160–2170. [[CrossRef](#)]
3. Bracci, S.; Iannaccone, R.; Magrini, D. The application of multi-band imaging integrated with non-invasive spot analyses for the examination of archaeological stone artefacts. *Conserv. 360°* **2020**, *1*, 141–160. Available online: https://monografias.editorial.upv.es/index.php/con_360/article/view/71 (accessed on 27 September 2023).
4. Aggelakopoulou, E.; Sotiropoulou, S.; Karagiannis, G. Architectural Polychromy on the Athenian Acropolis: An in situ non-invasive analytical investigation of the colour remains. *Heritage* **2022**, *5*, 756–787. [[CrossRef](#)]
5. Bourgeois, B.; Verri, G.; Jeamment, V. Color and Light: A Hellenistic Terracotta Figurine of a Maenad from Myrina. *Heritage* **2023**, *6*, 3005–3024. [[CrossRef](#)]
6. Pucci, E.; Cagnini, A.; Galeotti, M.; Salvadori, B. Prime indagini su opere bronzee da Pompei. Nuovi dati sulla policromia antica. *OPD Restauro* **2020**, *32*, 88–99.

7. Mathis, F.; Salomon, J.; Pagès-Camagna, S.; Dubus, M.; Robcis, D.; Aucouturier, M.; Descamps, S.; Delange, E. Corrosion patina or intentional patina: Contribution of non-destructive analyses to the surface study of copper-based archaeological objects. In *Corrosion of Metallic Heritage Artefacts*; European Federation of Corrosion (EFC) Series; Dillmann, P., Béranger, G., Piccardo, P., Matthiesen, H., Eds.; Woodhead Publishing: Cambridge, UK, 2007; pp. 219–238.
8. Scott, D.A. *Copper and Bronze in Art: Corrosion, Colorants, Conservation*; Getty Conservation Institute: Los Angeles, CA, USA, 2002.
9. Giunlia-Mair, A. Das Krokodil und Amenemhat III aus el-Faiyum. *Antike Welt* **1996**, *27*, 313–321.
10. Giunlia-Mair, A. Development of artificial black patina on Mycenaean metal finds. *Surf. Eng.* **2013**, *26*, 99–100.
11. Mathis, F.; Robcis, D.; Borel, T.; Aucouturier, M.; Descamps, S. Laboratory investigation of inlays and surface treatments for the decoration of copper-base alloy objects from the imperial Roman period. In Proceedings of the 34th International Symposium on Archaeometry, Zaragoza, Spain, 3–7 May 2004; pp. 201–208.
12. Mathis, F.; Descamps, S.; Robcis, D.; Aucouturier, M. Original surface treatment of copper alloy in ancient Roman Empire: Chemical patination on a Roman strigil. *Surf. Eng.* **2005**, *21*, 346–351. [[CrossRef](#)]
13. Craddock, P.; Giunlia-Mair, A. Hsmn-Km, Corinthian bronze, Shakudo: Black-patinated bronze in the ancient world. In *Metal Plating and Patination*; La Niece, S., Craddock, P., Eds.; Butterworth: London, UK, 1993; pp. 101–127.
14. Pitthard, V.; Stone, R.; Stanek, S.; Griesser, M.; Gersch, C.K.; Hanzer, H. Organic patinas on Renaissance and Baroque bronzes—Interpretation of compositions of the original patination by using a set of simulated varnished bronze coupons. *J. Cult. Herit.* **2011**, *12*, 44–53. [[CrossRef](#)]
15. Stone, R.E. Organic Patinas on Small Bronzes of the Italian Renaissance. *Metrop. Mus. J.* **2010**, *45*, 107–124. [[CrossRef](#)]
16. Basso, E.; Pozzi, F.; Day, J.; Borsch, L. Unmasking a wild man: Scientific analysis of Bertoldo di Giovanni’s Shield Bearer in the Frick Collection. *Herit. Sci.* **2020**, *8*, 109–121. [[CrossRef](#)]
17. Degano, I.; Modugno, F.; Colombini, M.P. Characterisation of organic patinas on indoor bronze sculptures. In Proceedings of the Art’11 10th International Conference on Non-Destructive Investigations and Microanalysis for the Diagnostics and Conservation of Cultural and Environmental Heritage, Florence, Italy, 13–15 April 2011.
18. Boon, J.; van Langh, R. Comprehensive studies of patinas on Renaissance bronze statuettes with laboratory, synchrotron and neutron aided techniques. In Proceedings of the ICOM Committee for Conservation 17th Triennial Meeting, Melbourne, Australia, 19–23 September 2014.
19. Darque-Ceretti, E.; Felder, E.; Aucouturier, M. Foil and leaf gilding on cultural artifacts: Forming and adhesion. *Matéria* **2011**, *16*, 540–559. [[CrossRef](#)]
20. Darque-Ceretti, E.; Aucouturier, M. Gilding for Matter Decoration and Sublimation. A brief history of the artisanal technical know-how. In Proceedings of the InART’13—1st International Conference on Innovation in Art Research and Technology, Evora, Portugal, 10–13 July 2013.
21. Oddy, W.A. A History of gilding with particular reference to statuary. In *Gilded Metals. History, Technology and Conservation*; Drayman-Weisser, T., Ed.; Archetype Publications: London, UK, 2000; p. 1.
22. Lins, A. Gilding Techniques of the Renaissance and after. In *Gilded Metals. History, Technology and Conservation*; Drayman-Weisser, T., Ed.; Archetype Publications: London, UK, 2000; p. 241.
23. Brepohl, E. *The Theory and Practice of Goldsmithing*; McCreight, T., Ed.; Brynmorgen Press: Portland, ME, USA, 2001.
24. Oddy, W.A. Gilding through the ages. *Gold Bull.* **1981**, *14*, 75–79. [[CrossRef](#)]
25. Selwyn, L. Corrosion Chemistry of Gilded Silver and Copper. In *Gilded Metals. History, Technology and Conservation*; Drayman-Weisser, T., Ed.; Archetype Publications: London, UK, 2000; p. 21.
26. Yriarte, C. Journal d’un sculpteur Florentin au XVe siècle: Livre de souvenirs de Maso di Bartolommeo, dit Masaccio, manuscrits conservés à la bibliothèque de Prato et à la Magliabecchiana de Florence. *J. Rothschild Ed.* **1894**, 49–53.
27. Madariaga, J.M. Analytical chemistry in the field of cultural heritage. *Anal. Methods* **2015**, *7*, 4848–4876. [[CrossRef](#)]
28. Shugar, A.N.; Mass, J.L. *Handheld XRF for Art and Archaeology*; Leuven University Press: Leuven, Belgium, 2012; p. 480.
29. Brocchieri, J.; Scialla, E.; Manzone, A.; Graziano, G.O.; D’Onofrio, A.; Sabbarese, C. An analytical characterization of different gilding techniques on artworks from the Royal Palace (Caserta, Italy). *J. Cult. Herit.* **2022**, *57*, 213–225. [[CrossRef](#)]
30. Derrick, M.; Stulik, D.; Landry, J.M. *Infrared Spectroscopy in Conservation Science. Scientific Tools for Conservation*; J. Paul Getty Trust: Los Angeles, CA, USA, 2000.
31. Figueiredo, E.; Silva, R.J.C.; Araújo, M.F.; Senna-Martinez, J.C. Identification of ancient gilding technology and Late Bronze Age metallurgy by EDXRF, Micro-EDXRF, SEM-EDS and metallographic techniques. *Microchim. Acta* **2010**, *168*, 283–291. [[CrossRef](#)]
32. Gianoncelli, A.; Kourousias, G. Limitations of portable XRF implementations in evaluating depth information: An archaeometric perspective. *Appl. Phys. A* **2007**, *89*, 857–863. [[CrossRef](#)]
33. Gigante, G.E.; Ridolfi, S. *X-ray Techniques and X-ray Fluorescence with Portable Systems*; Varella, E.A., Ed.; Conservation Science for the Cultural Heritage, Lecture Notes in Chemistry 79; Springer: Berlin/Heidelberg, Germany, 2013; pp. 91–161.
34. Scott, D.A.; Schwab, R. *Metallography in Archaeology and Art*; Springer: Cham, Switzerland, 2019.
35. La Russa, M.F.; Ruffolo, S.A.; Barone, G.; Crisci, G.M.; Mazzoleni, P.; Pezzino, A. The use of FTIR and micro-FTIR spectroscopy: An example of application to Cultural Heritage. *Int. J. Spectr.* **2009**, *2009*, 893528. [[CrossRef](#)]
36. Monico, L.; Rosi, F.; Miliani, C.; Daveri, A.; Brunetti, B.G. Non invasive identification of metal-oxalate complexes on polychrome artwork surfaces by reflection mid-infrared spectroscopy. *Spectrochim. Acta Part A Mol. Biomol. Spectrosc.* **2013**, *116*, 270–280. [[CrossRef](#)] [[PubMed](#)]

37. Frost, R.L. Raman spectroscopy of natural oxalates. *Anal. Chim. Acta* **2004**, *517*, 207–214. [[CrossRef](#)]
38. Martens, W.N.; Frost, R.L.; Williams, P. Raman and infrared spectroscopic study of the basic copper chloride minerals: Implications for the study of the copper and brass corrosion and “bronze disease”. *Neues Jahrb. Mineral. Abh.* **2003**, *178*, 197–215. [[CrossRef](#)]
39. Frost, R.L.; Yang, J.; Ding, Z. Raman and FTIR spectroscopy of natural oxalates: Implications for the evidence of life on Mars. *Chin. Sci. Bull* **2003**, *48*, 1844–1852. [[CrossRef](#)]
40. Van der Weerd, J.; Van Loon, A.; Boon, J.J. FTIR studies of the effects of pigments on the aging of oil. *Stud. Conserv.* **2005**, *50*, 3–22. [[CrossRef](#)]
41. Vetter, W.; Latini, I.; Schreiner, M. Azurite in medieval illuminated manuscripts: A reflection-FTIR study concerning the characterization of binding media. *Herit. Sci.* **2019**, *7*, 21. [[CrossRef](#)] [[PubMed](#)]
42. Filopoulou, A.; Vlachou, S.; Boyatzis, S.C. Fatty Acids and Their Metal Salts: A Review of Their Infrared Spectra in Light of Their Presence in Cultural Heritage. *Molecules* **2021**, *26*, 6005. [[CrossRef](#)] [[PubMed](#)]
43. Robinet, L.; Corbeil, M.C. The characterization of metal soaps. *Stud. Conserv.* **2003**, *48*, 23–40. [[CrossRef](#)]
44. Otero, V.; Sanches, D.; Montagner, C.; Vilarigues, M.; Carlyle, L.; Lopes, J.A.; Melo, M.J. Characterisation of metal carboxylates by Raman and infrared spectroscopy in works of art. *J. Raman Spectrosc.* **2014**, *45*, 1197–1206. [[CrossRef](#)]
45. Pellegrini, D.; Duce, C.; Bonaduce, I.; Biagi, S.; Ghezzi, L.; Colombini, M.P.; Tinè, M.R.; Bramanti, E. Fourier transform infrared spectroscopic study of rabbit glue/inorganic pigments mixtures in fresh and aged reference paint reconstructions. *Microchem. J.* **2016**, *124*, 31–35. [[CrossRef](#)]
46. Guglielmi, V.; Andreoli, M.; Comite, V.; Baroni, A.; Fermo, P. The combined use of SEM-EDX, Raman, ATR-FTIR and visible reflectance techniques for the characterisation of Roman wall painting pigments from Monte d’Oro area (Rome): An insight into red, yellow and pink shades. *Environ. Sci. Pollut. Res.* **2022**, *29*, 29419–29437. [[CrossRef](#)]
47. Müller, C.; Pejčić, B.; Esteban, L.; Delle Piane, C.; Raven, M.; Mizaikoff, B. Infrared Attenuated Total Reflectance Spectroscopy: An Innovative Strategy for Analyzing Mineral Components in Energy Relevant Systems. *Sci. Rep.* **2014**, *4*, 6764. [[CrossRef](#)] [[PubMed](#)]
48. Ellerbrock, R.; Stein, M.; Schaller, J. Comparing amorphous silica, short-range-ordered silicates and silicic acid species by FTIR. *Sci. Rep.* **2022**, *12*, 11708. [[CrossRef](#)]
49. Bordignon, F.; Postorino, P.; Dore, P.; Laurenzi Tabasso, M. The Formation of Metal Oxalates in the Painted Layers of a Medieval Polychrome on Stone, as Revealed by Micro-Raman Spectroscopy. *Stud. Conserv.* **2008**, *53*, 158–169. [[CrossRef](#)]
50. de Viguerie, L.; Payard, P.A.; Portero, E.; Walter, P.; Cotte, M. The drying of linseed oil investigated by Fourier transform infrared spectroscopy: Historical recipes and influence of lead compounds. *Prog. Org. Coat.* **2016**, *93*, 46–60. [[CrossRef](#)]
51. Costagliola, P.; Benvenuti, M.; Chiarantini, L.; Bianchi, S.; Di Benedetto, F.; Paolieri, M.; Rossato, L. Impact of ancient metal smelting on arsenic pollution in the Pecora River Valley, Southern Tuscany, Italy. *Appl. Geochem.* **2008**, *23*, 1241–1259. [[CrossRef](#)]
52. Van Langh, R.; James, J.; Burca, G.; Kockelmann, W.; Zhang, S.Y.; Lehmann, E.; Estermanne, M.; Pappot, A. New insights into alloy compositions: Studying Renaissance bronze statuettes by combined neutron imaging and neutron diffraction techniques. *J. Anal. At. Spectrom.* **2011**, *26*, 949. [[CrossRef](#)]
53. Bewer, F.G. A Study of the Technology of Renaissance Bronze Statuettes. Ph.D. Thesis, University of London, London, UK, 1996.
54. Radepon, M.; Coquinot, Y.; Janssens, K.; Ezrati, J.-J.; de Nolf, W.; Cotte, M. Thermodynamic and experimental study of the degradation of the red pigment mercury sulfide. *J. Anal. At. Spectrom.* **2015**, *30*, 599–612. [[CrossRef](#)]
55. Anaf, W.; Janssens, K.; De Wael, K. Formation of Metallic Mercury During Photodegradation/Photodarkening of α -HgS: Electrochemical Evidence. *Angew. Chem. Int. Ed.* **2013**, *52*, 12568–12571. [[CrossRef](#)]
56. Available online: <https://www.youtube.com/watch?v=B4fvZNPZjvI> (accessed on 14 February 2024).

Disclaimer/Publisher’s Note: The statements, opinions and data contained in all publications are solely those of the individual author(s) and contributor(s) and not of MDPI and/or the editor(s). MDPI and/or the editor(s) disclaim responsibility for any injury to people or property resulting from any ideas, methods, instructions or products referred to in the content.